ACS Catalysis

pubs.acs.org/acscatalysis

Research Article

Elucidating the Oxygen Activation Mechanism on Ceria-Supported Copper-Oxo Species Using Time-Resolved X-ray Absorption Spectroscopy

Olga V. Safonova,* Alexander Guda, Yury Rusalev, René Kopelent, Grigory Smolentsev, Wey Yang Teoh, Jeroen A. van Bokhoven, and Maarten Nachtegaal

Cite This: *ACS Catal.* 2020, 10, 4692–4701

Read Online

ABSTRACT: Copper-ceria finds applications in various energy-related and environmental catalysts. However, the versatile structure and complex redox activity of this material entangle uncovering structure−activity relationships and distinguishing active species from spectators. In this work, we monitored the dynamic structure of the active sites in a catalyst containing highly dispersed copper-oxo species on ceria during low-temperature CO oxidation using time-resolved X-ray absorption spectroscopy. We quantitatively demonstrate that the CO oxidation mechanism below 90 °C involves an oxygen intermediate strongly bound to the active sites as well as the redox activity of Cu^{2+}/Cu^{+} and Ce^{4+}/Ce^{3+} couples. The redox activity of cerium is much lower than that of copper; however, both metals change their oxidation states in concert, indicating that oxygen activation involves copper−oxo species in close interaction with ceria. In addition to short-lived Cu^{+} and Ce^{3+} intermediates that are generated in the CO oxidation cycle, long-lived Cu^{+} and Ce^{3+} species appear in the catalyst under the working conditions. We demonstrate that they do not participate in the main low-temperature CO oxidation mechanism, which is mediated by a strongly bound oxygen intermediate. Finally, our results confirm the high potential of element-specific time-resolved X-ray spectroscopy methods combined with a non-steady-state experimental strategy to uncover the mechanisms of catalytic processes in complex multicomponent systems.

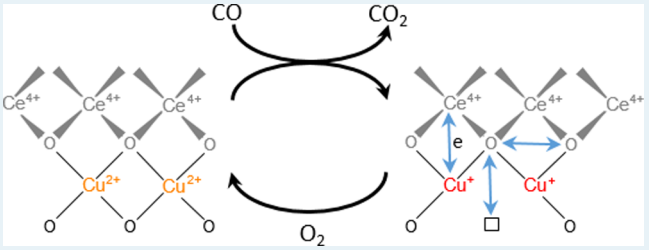

KEYWORDS: *copper-ceria, oxygen activation mechanism, CO oxidation, operando spectroscopy, time-resolved XAS, non-steady-state kinetics*

1. INTRODUCTION

Copper-ceria ($Cu\text{-}CeO_2$) is one of the most versatile alternatives to precious metal catalysts[1] with wide ranging applications that include the water-gas shift (WGS) reaction,[2,3] methanol synthesis,[4] oxidation and preferential oxidation of CO and volatile organic carbons,[5−7] and the reduction of nitrogen oxides (NO_x).[8−10] The versatility of the catalyst can be traced back to the dynamic and highly dispersed nature of the copper species on the ceria surface, giving rise to interesting, albeit moderately understood, redox properties. Furthermore, the synergetic chemical and electronic interactions between copper and ceria have been found to be favorable in catalyzing many of the surface reactions as mentioned above.

Under oxidizing conditions and at low loading, the copper species on ceria tend to be stabilized as cationic monomers and oligomers. However, on subjection to reducing conditions above 200 °C, the copper species segregate into two-dimensional, partially metallic nanoparticles.[3,11,12] In fact, both copper and cerium can vary their oxidation states under conditions of a specific catalytic process.[3,4,13−20] Although highly beneficial in mediating surface reactions, the structural and electronic versatility of $Cu\text{-}CeO_2$ represents a great spectroscopic challenge for elucidating the catalytic mechanisms at the atomic scale. Given its stoichiometric simplicity, CO oxidation is a well-adopted model reaction to probe the catalytic oxidation mechanisms because the limited intermediate pathways allow for obtaining an unobscured view in interpreting the mechanistic principles. In addition, this reaction has wide implications for some of the most fundamental reactions, including WGS and syngas conversions, exhaust treatment and air pollution mitigation, and the purification of hydrogen (i.e., preferential oxidation of CO traces).

Prior kinetics studies on CO oxidation over $Cu\text{-}CeO_2$ found that the low-temperature reactivity is similar in the absence or excess of hydrogen.[5,7,21,22] The high selectivity for CO oxidation

Received: February 1, 2020
Revised: March 19, 2020
Published: March 25, 2020

has been explained as due to the preferential adsorption of CO on copper sites.[17] The reaction order with respect to CO decreases from one to zero with increasing CO concentration, suggesting an equilibrium coverage of the active sites by CO during CO oxidation. The reaction order with respect to oxygen is typically close to zero (±0.15), which indicates that the majority of oxygen intermediates participating in the reaction are strongly bound to the surface.[5] Evidence for a Mars−van Krevelen (MvK) mechanism of CO oxidation was found in transient experiments through the observation of significant CO conversion in the absence of gas-phase oxygen.[21,23] At the same time, other mechanisms of CO oxidation involving weakly bound oxygen species, for example, peroxide species activated on Cu^{+},[24,25] could not be fully excluded on the basis of kinetics experiments alone.

The CO oxidation mechanism at the atomic scale remains uncertain due to the coexistence of various oxidation states of copper and cerium in the catalyst structure, which depends on the synthesis method, copper loading, reaction conditions, and the pretreatment history. In situ infrared spectroscopy studies by Gamarra et al.[26] and Polster et al.[21] demonstrated a correlation between the CO oxidation activity of different Cu-CeO_2 catalysts and the intensity of the Cu^{+} carbonyl peak. These results suggest that CO is either directly activated on Cu^{+} to participate in the CO oxidation reaction or Cu^{+} carbonyl species appears after reduction of Cu^{2+} to Cu^{+} during the CO oxidation cycle. It is also not certain which redox couple compensates the negative charge created after the removal of lattice oxygen according to the MvK mechanism. Several possibilities were suggested in the literature, including Cu^{2+}/Cu^{+},[13−17] Ce^{4+}/Ce^{3+},[5,13] Cu^{+}/Cu^{0},[16] and Cu^{3+}/Cu^{2+} [18] redox couples. A "synergetic" mechanism considering fast O^{2-} diffusion from cerium to the copper sites, where CO oxidation takes place, was also proposed.[16] In situ and operando experiments using X-ray absorption spectroscopy (XAS),[15,27,28] and infrared[17,21,26] and electron paramagnetic resonance (EPR)[16] spectroscopies demonstrate that both copper and cerium can change their oxidation states under relevant conditions and thus can potentially participate in the oxygen activation mechanism. However, the rates of oxidation and reduction of copper and cerium sites were never quantified and correlated to the CO_2 formation rate,[29] making the discrimination between possible mechanisms and verification of species involved in the catalytic cycle impossible.

In our previous works,[30,31] we demonstrated using transient oxygen cutoff experiments (cycling between a mixture of CO and oxygen and one of CO) combined with operando time-resolved X-ray emission spectroscopy methods that the Ce^{3+} formation rate is kinetically coupled to the rate-determining step of low-temperature CO oxidation on a Pt/CeO_2 catalyst. These studies indicated that lattice oxygen at the metal−support interface reacts with CO adsorbed on platinum, generating two Ce^{3+} ions, which are rapidly reoxidized to Ce^{4+} in the presence of gas-phase oxygen. Here we used a similar approach to clarify the mechanism of oxygen activation on highly dispersed copper−oxo species on ceria at low temperature, i.e. combining transient oxygen cutoff experimentation with X-ray absorption spectroscopy (XAS) at the Cu K and Ce L_3 edges. Our results quantitatively demonstrate for the first time the following.

(i) CO oxidation below 90 °C is mediated by a strongly bound oxygen intermediate and by Cu^{2+}/Cu^{+} and Ce^{4+}/Ce^{3+} redox couples.

(ii) The redox activity of cerium is much lower than that of copper; however, both metals change their oxidation states in concert, indicating that oxygen activation involves copper-oxo species in close interaction with ceria.

(iii) Long-lived Cu^{+} and Ce^{3+} species exist on the surface during low-temperature CO oxidation, but they do not participate in the main reaction mechanism.

2. EXPERIMENTAL SECTION

For this study, we selected a well-established Cu-CeO_2 catalyst, containing highly dispersed copper-oxo species which is highly active for CO oxidation, prepared by the flame spray pyrolysis method.[12] This Cu-CeO_2 (4 wt % Cu) catalyst has a specific surface area of 93 m^2/g, and details about its synthesis, characterization, and activity assessments can be found elsewhere.[12] X-ray photoelectron spectroscopy (XPS), X-ray diffraction (XRD), transmission electron microscopy (TEM), Raman spectroscopy, electron paramagnetic resonance (EPR) spectroscopy, and elemental analysis suggested preferential segregation of copper oligomers of different nuclearity on the surface of ceria without the formation of crystalline CuO_x phases. Systematic variation of the copper concentration between 0.5 and 12 wt % demonstrated a maximum of preferential CO oxidation activity for 4 wt % of copper coinciding with the strongest signal for Cu^{2+} dimers in EPR.

In this work, we characterized this catalyst by scanning transmission electron microscopy (STEM) and in situ/operando XAS. STEM combined with energy-dispersive X-ray spectroscopy (EDXS) was performed on a Talos microscope (FEI) with a high brightness field emission gun operated at an acceleration potential of 200 kV. Four EDX detectors allowed recording EDXS maps within 10−20 min.

The scheme of the setup for the in situ/operando time-resolved XAS studies used in our work is shown in Figure 1. A

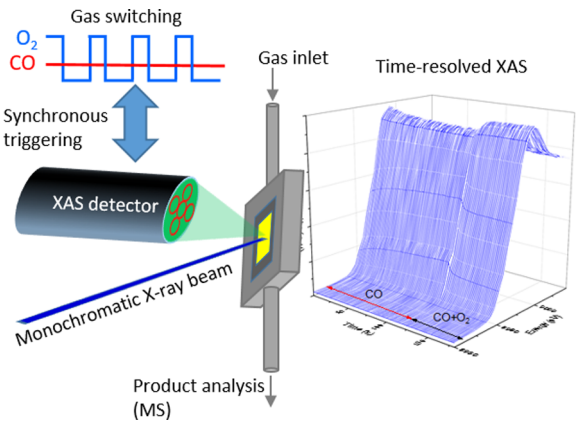

Figure 1. Scheme of the experimental setup for in situ/operando time-resolved XAS studies of heterogeneous catalysts in a plug-flow reactor cell.

sieved fraction of 4 wt % Cu-CeO_2 catalyst (12−65 mg) containing 100−150 μm particles was loaded in a plug-flow reactor cell.[32] The catalyst was precalcined in 4% oxygen at 300 °C. The gas flow was passing through the catalyst in a vertical direction. We used two cartridge heaters (Tuerk-Hillinger) to control the cell temperature (24−400 ± 1 °C). The temperature of the catalyst bed was measured by an additional thermocouple placed in the middle of the catalyst bed. We used 150 μm thick graphite foils as X-ray windows. The gas-feeding setup consisted

https://dx.doi.org/10.1021/acscatal.0c00551
ACS Catal. 2020, 10, 4692−4701

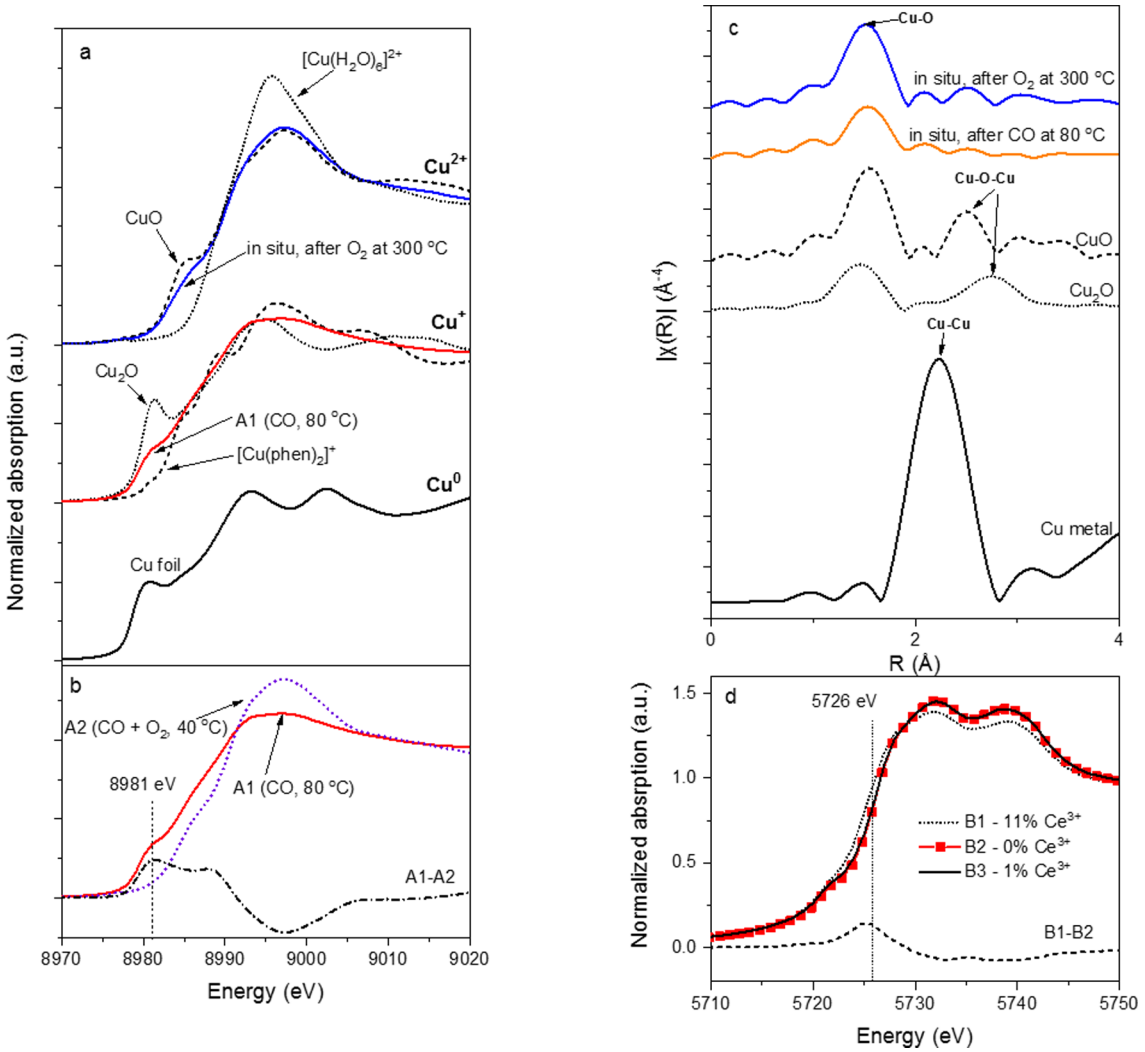

Figure 2. (a) Cu K edge XANES spectra of 4 wt % Cu/CeO_2 catalyst after calcination in 4% oxygen at 300 °C and in 1% CO at 80 °C in comparison to Cu^{2+}, Cu^+, and Cu^0 references. (b) Cu K edge XANES spectra of 4 wt % Cu/CeO_2 catalyst in A1 and A2 states and the A1−A2 difference spectrum. (c) Fourier-transformed Cu K edge EXAFS spectra of 4 wt % Cu/CeO_2 catalyst after calcination in 4% oxygen at 300 °C and after exposure to 1% CO at 80 °C in comparison to the corresponding spectra for CuO, Cu_2O, and Cu. (d) Ce L_3 edge XANES spectra of 4 wt % Cu/CeO_2 catalyst in 1% CO and 4% oxygen at 66 °C (B3 reference) together with the reference spectra of 1.5 wt % Pt/CeO_2 catalyst in 1% CO (B1 reference) and in 4% oxygen (B2 reference) and the B1−B2 difference.

of mass flow controllers (El-Flow, Bronkhorst) connected to gas bottles of 5% CO in argon (CO 4.7 purity, argon 5.0 purity), 21% oxygen in argon (oxygen 4.5 purity, argon 5.0 purity), and argon (4.8 purity). During transient experiments, we used two three-way solenoid valves (Parker) to switch between two gas mixtures (1% CO and 4% oxygen in argon vs 1% CO in argon) passing through the cell and bypass with a constant flow (50 mL/min). The pressure difference between the cell and the bypass was less than 100 mbar, and we further reduced it to 2 mbar by a needle valve back-pressure regulator placed at the bypass. We analyzed the residual gas at the cell exit using a mass spectrometer (OmniStar GSD 320, Pfeiffer) and monitored the mass to charge (m/z) ratios of 28, 32, 40, and 44 corresponding to CO, oxygen, argon, and CO_2, respectively. We quantified the CO conversion using the CO_2 signal (m/z 44) divided by that of argon (m/z 40). A 1% CO_2 in argon gas mixture was used for the calibration of the mass spectrometer.

During kinetic tests, we analyzed the catalytic activity of 4 wt % Cu-CeO_2 in a flow of gas mixtures containing 0.25−4% CO and 3−16% oxygen at 39−90 °C. The CO conversion was typically kept below 30% to ensure uniform reactivity of the whole catalyst bed. The state of the catalyst was probed by XAS in the middle of the catalyst bed. Figure S1 demonstrates how fast the gas atmosphere in the reactor cell can be exchanged. While switching between two gas mixtures, pure argon versus 10% krypton in argon, we monitored the rate of krypton removal from the reactor following the decay of the m/z 86 signal of krypton. The exponential decay fit of the resulting curve demonstrates a characteristic time of 1.4 s.

2.1. Time-Resolved X-ray Absorption Spectroscopy. The XAS experiments at the Ce L_3 and Cu K edges were performed at the SuperXAS beamline of the Swiss Light Source (PSI, Villigen, Switzerland). The incident photon beam was selected by a Si (111) channel-cut monochromator from the polychromatic beam coming from a 2.9 T superbend magnet. The rejection of higher harmonics and the collimation were achieved by a silicon-coated collimating mirror at 2.5 mrad located before the monochromator, while focusing was achieved by a rhodium-coated torroidal mirror at 2.5 mrad. For the detection of Ce L_3 and Cu K-edge XAS, we calibrated the

https://dx.doi.org/10.1021/acscatal.0c00551
ACS Catal. 2020, 10, 4692−4701

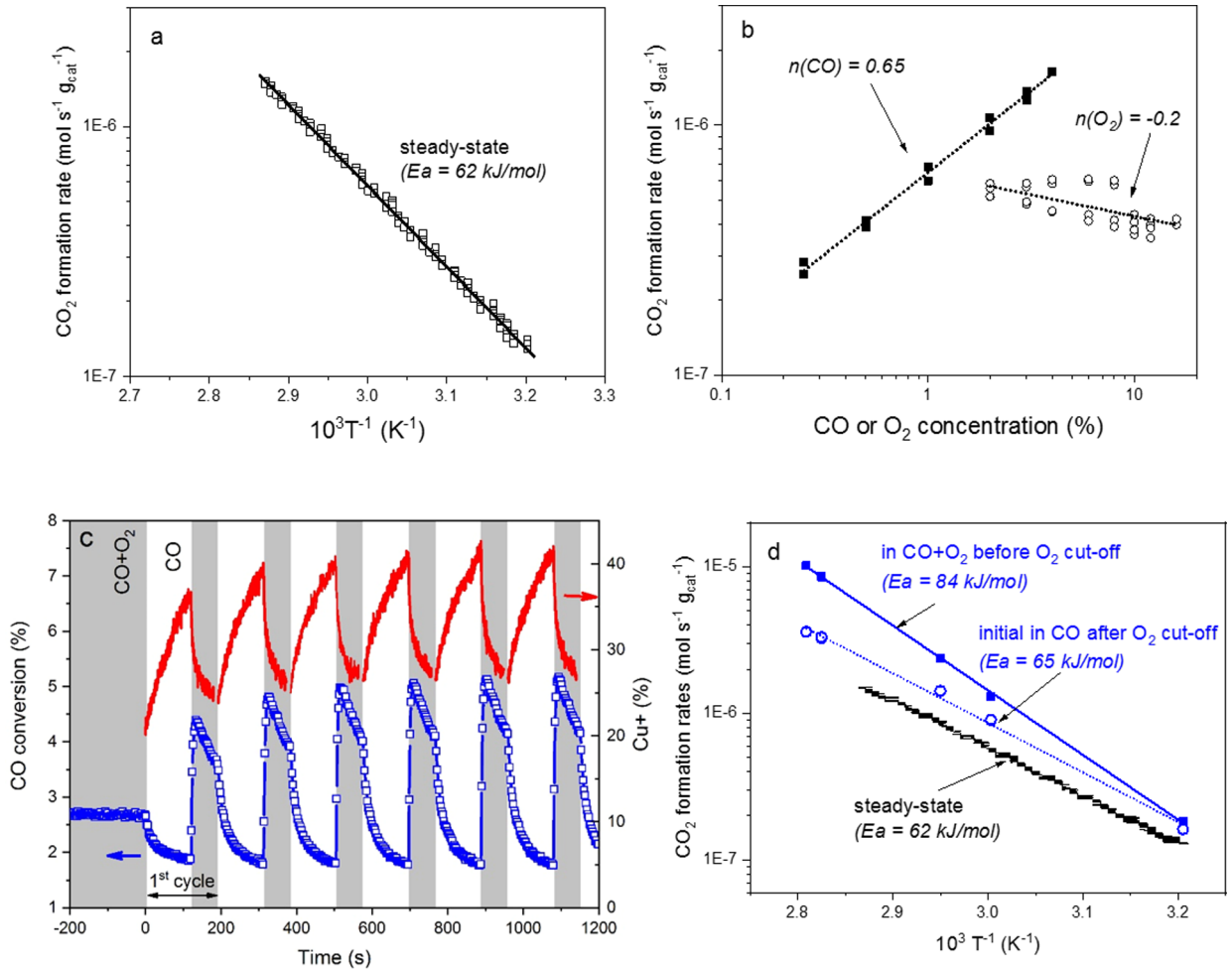

Figure 3. (a) Steady-state CO oxidation rate over 4 wt % Cu/CeO_2 catalyst as a function of temperature. (b) Steady-state CO oxidation rate over 4 wt % Cu/CeO_2 catalyst as a function of CO and oxygen concentrations. (c) Evolution of CO conversion and Cu^+ concentration during a repeated temporal oxygen cutoff experiment at 60 °C involving cycling between 1% CO (120 s) and 1% CO and 4% oxygen (60 s) after equilibration in 1% CO and 4% oxygen. Gray fields correspond to 1% CO and 4% oxygen; white fields correspond to 1% CO. (d) Comparison of CO_2 formation rates during the tenth cycle of oxygen cutoff experiments and under steady-state conditions.

beamline with vanadium (K edge at 5465 eV) and copper (K edge at 8979 eV) foils, respectively. The size of the X-ray beam on the sample was about 1.5 mm in the horizontal direction and 0.5 mm in the vertical direction with a total flux of about (3−7) × 10^{11} ph/s.

Cu foil, CuO, Cu_2O, and $Cu(NO_3)_2{\cdot}6H_2O$ standards were measured in transmission mode. Due to the strong X-ray absorption in the 4 wt % Cu-CeO_2 catalyst, in situ/operando experiments were performed in fluorescence mode (Figure 1). The fluorescence signal was detected with a five-element silicon drift detector (SGX) and processed by XIA electronics. We used titanium- and nickel-containing filters to suppress the elastic scattering while measuring the Ce Lα and Cu Kα fluorescence signals, respectively. To measure XAS with 0.5 s time resolution, we used the DXP-XMAP mapping mode of the XIA data acquisition system described in detail in our previous work.[33] For normalization of the fluorescence signal to the intensity of the incoming beam, we used an ionization chamber placed before the sample. For quantification of the Ce^{3+} concentration we used an additional reference sample (1.5 wt % Pt/CeO_2 catalyst described in detail elsewhere[30]). To compare the reactivities of cerium and copper, we performed similar in situ/operando experiments at the Ce L_3 and Cu K edges. Principal component and linear combination analyses were done using the Fitit software.[34,35]

To compare the local structure of copper in the Cu-CeO_2 catalyst to that of the reference samples, we pretreated the catalyst under specific conditions, cooled it down to 39−40 °C in the same gas atmospheres and measured in situ the extended X-ray absorption fine structure (EXAFS) spectra at the Cu K edge. We analyzed the EXAFS spectra using the Demeter software package[36] and fitted the Fourier-transformed k^3-weighted signal for k = 3−11 Å^{-1} with dk = 1 and R = 1−3 Å with dR = 0.5.

3. RESULTS AND DISCUSSION

3.1. State of Copper and Catalytic Activity. Figure 2a compares the Cu K edge XANES spectra of the Cu-CeO_2 catalyst calcined at 300 °C in 4% oxygen to those of various Cu^{2+}, Cu^+, and Cu^0 standards. The spectrum of the calcined catalyst closely resembles that of CuO, which has Cu^{2+} sites in square-planar oxygen coordination. By comparison, the Cu-$(NO_3)_2{\cdot}6H_2O$ standard containing Cu^{2+} cations in the distorted-octahedral environment of $[Cu(H_2O)_6]^{2+}$ demonstrates the absence of a shoulder at ca. 8985 eV (corresponding to the dipole-allowed 1s to 4p_z electronic transition) and has a

https://dx.doi.org/10.1021/acscatal.0c00551
ACS Catal. 2020, 10, 4692−4701

much higher white line peak at ca. 8996 eV. The absence of a peak at ca. 9016 eV for the 4 wt % Cu-CeO_2 catalyst is typical of highly dispersed Cu^{2+} sites on the surface of ceria crystallites.[26,37] Fitting of the Cu K-edge EXAFS spectrum of the catalyst (Figure 2c and Figure S2 and Table S1) indicates of on average ca. 3.9 oxygen neighbors around copper at a distance of 1.929 Å. This distance is slightly shorter in comparison to the Cu−O distances reported for CuO (1.95−1.96 Å) and similar to those reported for highly dispersed copper on ceria.[11,38,37,39] The second coordination shell around copper (Cu−O−Cu) can be fitted by 0.7 copper neighbor at ca. 2.87 Å (Table S1). This highly dispersed nature of copper oxo species on the ceria surface is in agreement with STEM images of the catalyst before and after operando experiments (Figure S3). Previously, EPR data suggested the predominant presence of Cu^{2+} dimers in this catalyst[12] that correlate well with the small number of copper neighbors in the second coordination shell of copper as estimated by EXAFS analysis. These results are furthermore in agreement with earlier works suggesting stabilization of highly dispersed Cu^{2+} species on the ceria surface under oxidizing conditions as described by the wetting phenomenon[11] that was confirmed theoretically.[18,20]

We also analyzed the Cu K edge XAS spectra of the Cu-CeO_2 catalyst upon exposure to CO at 80 °C (Figure 2a,c). Fitting of the Cu K edge EXAFS spectrum of the Cu-CeO_2 catalyst exposed to 1% CO at 80 °C and cooled to 39 °C under the same atmosphere (Figure S2 and Table S1) did not detect any Cu−Cu coordination corresponding to metallic copper. Such a neighboring shell at ca. 2.5 Å was observed in the literature for Cu-CeO_2 only after exposure to CO and hydrogen above 200 °C.[3,11,38] Interestingly, also the Cu−Cu scattering path detected for the oxidized catalyst disappears upon exposure to CO. We can suggest that removal of oxygen from the Cu−O−Cu ensemble increases the static disorder because copper atoms get an additional degree of freedom. This effect, however, can also be related to the k range of our EXAFS data being too short (up to 11 $Å^{-1}$), which is due to the general difficulties in measuring high-quality EXAFS data for a low concentration of the element of interest in a highly absorbing matrix, such as CeO_2. The number of oxygen neighbors around copper in the Cu-CeO_2 catalyst upon exposure to CO at 80 °C decreased to 2.5 without a significant change in the Cu−O bond length (1.94 Å). Such a coordination suggests a linear (2-fold) coordination of Cu^+ similar to that in Cu_2O, except that in Cu_2O the length of the Cu−O bonds is significantly shorter (1.85 Å). The Cu K edge XANES spectrum of the catalyst acquired in 1% CO at 80 °C (Figure 2a) resembles that of Cu_2O but has a smaller shoulder at the edge (at 8981 eV) corresponding to the 1s to $4p_z$ transition. The intensity of this shoulder increases for linearly coordinated Cu^+ sites due to a large contribution of the copper p_z orbital located perpendicularly to the O−Cu−O bond. Figure 2a further shows that in the spectrum of a Cu^+ complex with phenanthroline ($[Cu(phen)_2]^+$),[40] where copper is coordinated by four nitrogen ligands in a tetrahedral geometry, the aforementioned shoulder completely disappears. This happens since the p_z orbital is mixed with p_y and p_x orbitals and not separated energetically from the other p orbital manifolds. Thus, one may reasonably conclude that copper sites in the Cu-CeO_2 catalyst exposed to 1% CO at 80 °C are mainly in the Cu^+ state with a nonideal linear oxygen coordination. At this point, the presence of minor quantities of Cu^{2+} and Cu^0 cannot be excluded.

Figures 3a,b shows the results of kinetic characterization of the Cu-CeO_2 under steady-state CO oxidation conditions. The apparent activation energy measured in the temperature range of 39−75 °C is close to 62 kJ/mol (Figure 3a). The CO conversion increases as a function of CO concentration, and the reaction order with respect to CO measured at 64 °C in 4% of oxygen and 0.25−4% CO is close to 0.65 (Figure 3b). Changes in the oxygen concentration only weakly affect the CO conversion, while the reaction order with respect to oxygen at 64 °C in 1% CO and 3−16% oxygen is close to −0.2. These results suggest that, during CO oxidation, the active sites are only partially covered by CO, and this correlates with the relatively weak CO adsorption on an oxidized surface containing mainly Cu^{2+}. A slightly negative reaction order with respect to oxygen indicates that oxygen mildly poisons the sites for CO adsorption. Overall, the activity and kinetic parameters obtained in our study are similar to those reported in the literature for highly dispersed copper on ceria under similar reaction conditions.[5,21,22,38]

To uncover the involvement of the redox activity of copper and cerium in the mechanism of CO oxidation, we wanted to correlate the rates of CO_2 formation to the rates of oxidation and reduction of copper and cerium atoms in the Cu-CeO_2 catalyst. Therefore, we performed oxygen cutoff experiments[30] by first exposing the catalyst to 1% CO and 4% oxygen and then switching off the oxygen supply, leaving the catalyst in 1% CO. Doing so allows measuring the rates of formation and decay of copper and cerium intermediates. We repeated the experiments several times and at several temperatures below 90 °C. The experiments are given in Table S2. In the next sections we will discuss (i) the catalytic activity of the Cu-CeO_2 during oxygen cutoff experiments, (ii) time-resolved chemical speciation of copper and cerium, and finally (iii) the low-temperature CO oxidation mechanism that can be formulated on the basis of these experiments.

3.2. Catalytic Activity during Oxygen Cutoff Experiments. Figure 3c shows the evolution of CO conversion over the Cu-CeO_2 catalyst at 60 °C during six periodic oxygen cutoff cycles, which we performed after equilibration of the catalyst in a 1% CO and 4% oxygen gas mixture for ca. 2100 s. The changes in the Cu^+ concentration measured simultaneously using operando Cu K edge XANES are also shown (vide infra). The first cycle in Figure 3c differs from the others, but afterward both CO conversion and Cu^+ concentration evolve reproducibly. For the first and the tenth oxygen cutoff cycles, we evaluated two parameters: (i) the rate of CO_2 formation in the 1% CO and 4% oxygen flow just before switching off the oxygen supply and (ii) the initial CO_2 formation rate in the absence of oxygen. The results are given in Table S2. To estimate the initial reaction rate in 1% CO, we integrated the corresponding CO_2 formation rate during 120 s exposure in 1% CO, fitted the resulting curve with an exponential decay function, and determined the first derivative at the initial condition right after the switch (Figure S4). Figure 3d compares these rates (evaluated from the tenth cycle) to the steady-state CO_2 formation rate for the same catalyst, already shown in Figure 3a. The initial rate of CO_2 formation in 1% CO is only about 1.5 times higher than the steady-state CO_2 formation rate and shows a similar apparent activation energy (ca. 62−65 kJ/mol). This suggests that CO oxidation involves a strongly bound oxygen intermediate, which also oxidizes CO in the absence of oxygen in the gas phase. At the same time, during oxygen cutoff cycles we observed that the CO_2 formation rate in the presence of oxygen is systematically higher than that under the steady-state conditions and has a

https://dx.doi.org/10.1021/acscatal.0c00551
ACS Catal. 2020, 10, 4692−4701

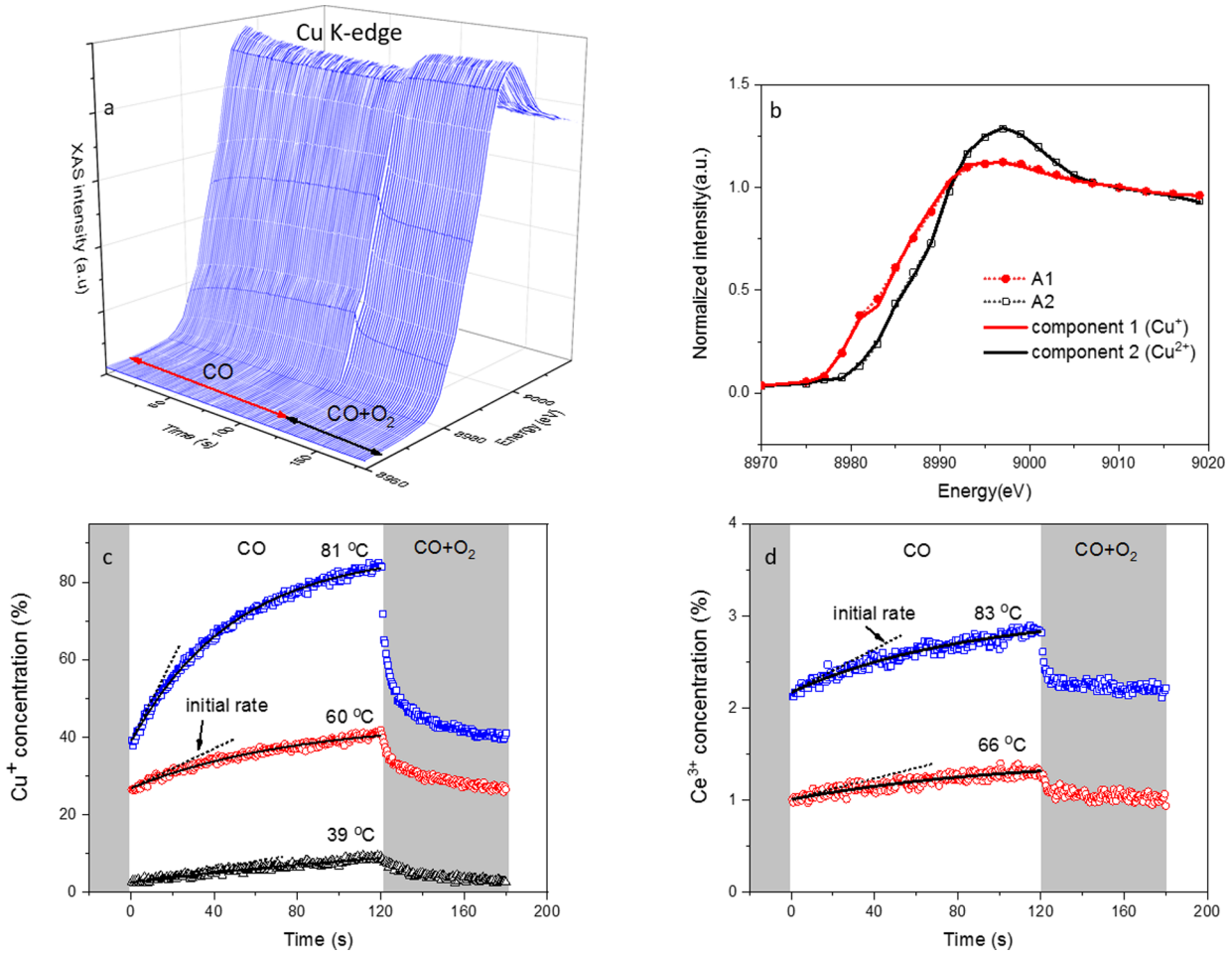

Figure 4. (a) Evolution of Cu K edge XANES for 4 wt % Cu/CeO_2 catalyst during periodic oxygen-cutoff experiments, where at each energy point the catalyst was exposed to 1% CO (120 s) and then to 1% CO and 4% oxygen (60 s). (b) Comparison of Cu K edge XANES spectra for 4 wt % Cu/CeO_2 catalyst in A1 and A2 states with the components 1 and 2 obtained by the PCA analysis of the time-resolved spectra. (c) Evolution of Cu^+ concentration in 4 wt % Cu/CeO_2 catalyst during oxygen cutoff experiments at 39, 60, and 81 °C (during the tenth cycle). Solid lines show the fits of Cu^+ concentration increase in 1% CO by single exponential decay functions and dashed lines indicate the initial Cu^+ formation rates at the moment of oxygen cutoff. (d) Evolution of Ce^{3+} concentration in 4 wt % Cu/CeO_2 catalyst during oxygen cutoff experiments at 66 and 83 °C (average of 19 cycles). Solid lines show the fits of Ce^{3+} concentration increase in 1% CO by single-exponential decay functions, and dashed lines indicate the initial Ce^{3+} formation rates at the moment of oxygen cutoff.

higher apparent activation energy of 84 kJ/mol (Figure 3d). This is related to an activity spike appearing after pre-exposure of the catalyst to the reducing atmosphere of CO. The spike was most prominent at 80 °C (Figure S5) but gradually decreased at 60 °C (Figure S6) and almost disappeared at 39 °C (Figure S7). Moreover, during the oxygen cutoff cycles at 80 °C, we observed an increase in the catalyst bed temperature up to 86 °C upon switching on oxygen, which can partially explain the origin of the activity spike (Figure S5). Below 60 °C, the catalyst temperature was constant but its activity was still increasing after exposure in CO and then slowly decaying (Figure S8). Indications for an increased CO_2 formation rate after exposure of the Cu-CeO_2 catalysts to CO can be found in the literature,[17,23,41−43] where the release of carbonates and oxidation of carbonyls stored on the catalyst surface during pretreatment in CO can explain this effect.

We do not rule out, at this juncture, the possibility of an additional catalytic CO oxidation mechanism appearing in the catalyst upon the exposure in CO. It is known that CO is not bound well to Cu^{2+}; therefore, during CO oxidation on a preoxidized Cu-CeO_2 catalyst the reaction order in CO is high (Figure 3b). At the same time, CO adsorbs better on reduced Cu^+. Thus, a higher concentration of reduced copper could enhance CO adsorption and accelerate the catalytic process involving a strongly bound oxygen intermediate. However, we observed from the oxygen cutoff experiments that the rate of CO oxidation increases much more strongly in the presence than in the absence of oxygen (Figure 3d). Thus, an additional CO oxidation mechanism temporarily appearing after exposure of the catalyst in CO may involve rather weakly bound oxygen intermediates that are present on the surface in equilibrium with the gas-phase oxygen and disappear when the oxygen supply is cut off. For this mechanistic study, it is important that during oxygen-cutoff experiments the measurements of the initial rate of CO oxidation in the absence of oxygen and its apparent activation energy are similar to those observed for steady-state CO oxidation over the preoxidized Cu-CeO_2 catalyst.

3.3. Time-Resolved Chemical Speciation of Copper and Cerium. To quantify changes in the copper state in Cu-CeO_2 catalyst during oxygen-cutoff experiments as probed by the operando time-resolved Cu K edge XANES, we used the corresponding spectra of the catalyst measured under steady-

https://dx.doi.org/10.1021/acscatal.0c00551
ACS Catal. 2020, 10, 4692−4701

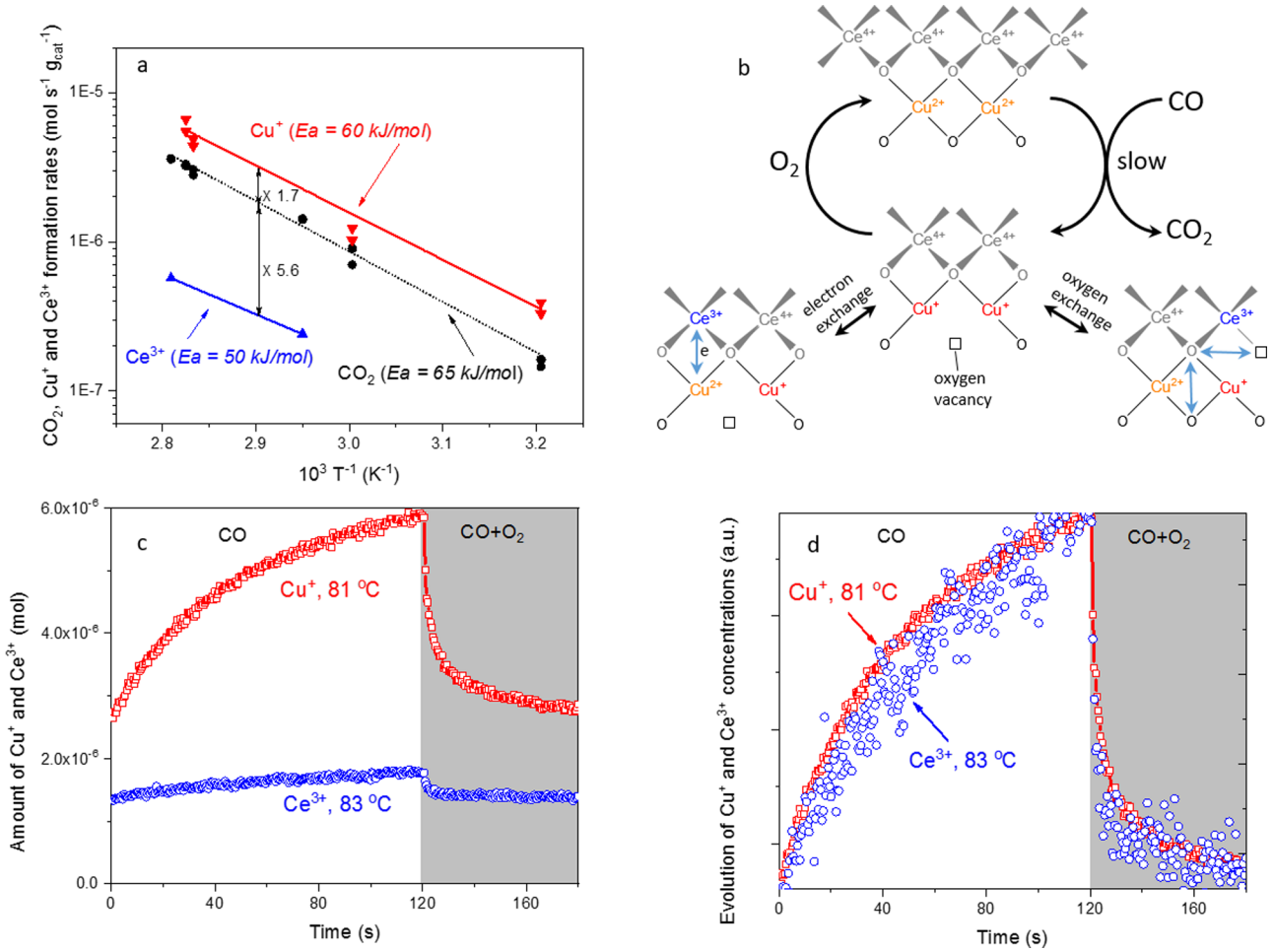

Figure 5. (a) Comparison of the initial rates of CO_2, Cu^+, and Ce^{3+} formation in 1% CO during oxygen-cutoff experiments at different temperatures. (b) Scheme explaining the redox activity of active sites during low-temperature CO oxidation on copper-ceria catalysts. (c) Evolution of absolute amounts of Cu^+ and Ce^{3+} in 4 wt % Cu/CeO_2 catalyst during oxygen-cutoff experiments at similar temperatures. (d) Evolution of Cu^+ and Ce^{3+} amounts in 4 wt % Cu/CeO_2 catalyst on relative scales.

state conditions, between the time-resolved experiments. Figure 2b shows such Cu K-edge XANES spectra of the Cu-CeO_2 catalyst in the most reduced state (A1 reference) and the most oxidized state (A2 reference) used for quantitative analysis. The A1 reference XANES spectrum was measured at 80 °C in 1% CO and the A2 reference at 39 °C in a flow of 1% CO and 4% oxygen. The Cu K edge XANES of A2 is very similar to that for the catalyst after calcination in 4% oxygen at 300 °C (Figure S9). As verified by XANES and EXAFS analyses (Figure 2 and Figure S2 and Table S1), the precalcined catalyst comprises mainly of Cu^{2+} species. Therefore, we assume that the A2 reference also corresponds to Cu^{2+}. We have also established above that the catalyst exposed to 1% CO at 80 °C (A1 reference) contains mainly Cu^+ species (Figure 2). This correlates to the literature suggesting that formation of Cu^0 in CO is not very probable for highly dispersed copper-ceria catalysts below 90 °C.[26,38,37] To confirm that the A1 reference does not contain significant amounts of Cu^0, we also analyzed the time-resolved Cu K edge XANES spectra of the Cu-CeO_2 catalyst during periodic oxygen-cutoff cycling at 81 °C by principal component analysis (PCA). Figure 4a shows the resulting 360 XANES Cu K edge spectra collected with 0.5 s time resolution. PCA revealed only two components, which perfectly match the spectra and the A1 and A2 references (Figure 4b and Figure S10). Thus, we finally assigned the A1 reference to the Cu^+ state. Consequently, we performed the majority of the time-resolved Cu K edge experiments at a fixed incident energy of 8981 eV, as it was sufficient for chemical speciation in a two-component system containing Cu^{2+} and Cu^+. The difference between the Cu K-edge XANES spectra of the A1 and A2 references indicates that 8981 eV is the optimal energy for quantification of Cu^+ and Cu^{2+} concentrations in this system. Further details about quantification of the Cu^+ concentration are given in the Supporting Information.

We applied a similar approach for time-resolved speciation of cerium using Ce L_3 edge XANES.[33] However, the concentration of Ce^{3+} in the Cu-CeO_2 catalyst under static conditions at the studied temperature range was too low to use these data for quantitative analysis. Therefore, as references, we used the Ce L_3-edge XANES spectra of a 1.5 wt % Pt/CeO_2 catalyst[30,44] measured previously in the same cell under static conditions at 150 °C in 1% CO (B1 reference containing 11% of Ce^{3+}) and in 4% oxygen (B2 reference containing no Ce^{3+}) shown in Figure 2d. Further details on quantification of the Ce^{3+} concentration are given in the Supporting Information. Considering the complexity of this analysis involving self-absorption correction, use of standards other than the catalyst itself, and averaging of XAS signals obtained during several gas switching cycles, we expect that the error bar on Ce^{3+} concentration can be as high as 100%. This would result in uncertainties of about a factor of 2 for

https://dx.doi.org/10.1021/acscatal.0c00551
ACS Catal. 2020, 10, 4692−4701

Ce^{3+} formation rates but would not affect the value of the corresponding apparent activation energy.

3.4. Mechanism of Low-Temperature CO Oxidation over Cu-CeO_2. Figure 4c compares the evolution of the Cu^+ concentration in the Cu-CeO_2 catalyst during oxygen cutoff experiments at different temperatures during the tenth cycle (the results of the first cycle are shown in Figure S13). Figure 4d summarizes the evolution of the Ce^{3+} concentration under similar conditions. Both Cu^+ and Ce^{3+} concentrations increase after oxygen cutoff to 1% CO and decrease again in 1% CO and 4% oxygen. The initial rates of Cu^+ and Ce^{3+} formation in CO are slower than their decay in CO and oxygen. This agrees with the kinetics experiments indicating that, under steady-state conditions, the active sites are largely covered by oxygen, leading to a low order of reaction with respect to oxygen. Some long-lived Cu^+ and Ce^{3+} species formed in CO tend to decay slowly in the presence of oxygen and their concentration is dependent on the temperature and pretreatment history (Table S2); they do not play any role in the activation of strongly bound oxygen intermediates.

To verify the involvement of Cu^{2+}/Cu^+ and Ce^{4+}/Ce^{3+} redox couples in the mechanism of low-temperature CO oxidation, we quantified the initial rates of Cu^+ and Ce^{3+} formation after oxygen cutoff. We fitted the Cu^+ and Ce^{3+} concentration profiles during 120 s in 1% CO by an exponential decay function (Figure 4c,d) and assigned the first derivatives of the resulting curves at the initial moment to the initial rates of Cu^+ and Ce^{3+} formation, respectively.[30] Figure 5a compares the resulting initial CO_2, Cu^+, and Ce^{3+} formation rates in CO. The Cu^+ formation rate is ca. 1.7 times higher than the CO_2 formation rate, while the Ce^{3+} formation rate is ca. 5.6 times lower than the CO_2 formation rate. Even when 2-fold uncertainties for Ce^{3+} formation rates are considered, Ce^{3+} forms much more slowly than CO_2. The stoichiometry of CO oxidation involving lattice oxygen (O^{2-}) implies that two electrons should be formed per one CO_2 molecule:

$$O^{2-} + CO = CO_2 + 2e \quad (1)$$

To fulfill the electron balance, these electrons should be transferred either on copper

$$Cu^{2+} + e = Cu^+ \quad (2)$$

or on cerium

$$Ce^{4+} + e = Ce^{3+} \quad (3)$$

A comparison of the initial rates (Figure 5a) suggests that the total number of electrons participating in reaction 1 is about 1.9 times higher than the number of CO_2 molecules, matching the stoichiometry of this reaction. About 91% of electrons were derived from the reduction of Cu^{2+} to Cu^+, while only 9% of them were derived from the reduction of Ce^{4+} to Ce^{3+}. Note that the latter process does not necessarily point to the direct oxidation of CO by the Ce^{4+}/Ce^{3+} couple, which would not take place in CO at such low temperatures.[45] Rather, Ce^{3+} species appear as the result of electron exchange between copper and cerium redox couples or/and lattice oxygen mobility between the neighboring sites schematically depicted in Figure 5b describing the mechanism. The effect is further verified in Figure 5c,d by comparing the kinetics of Cu^+ and Ce^{3+} formation and decay during oxygen cutoff experiments performed at similar temperatures on absolute and relative scales. On the absolute scale (Figure 5c), the more prominent increase in Cu^+ concentration in comparison with that of Ce^{3+} clearly confirms the above observation based on the initial rates. Importantly, when they are depicted on the relative scales, the kinetics of the redox transformations of both copper and cerium (Figure 5d) demonstrate excellent agreement. In other words, copper and cerium should be chemically interacting, forming the same active site. To the best of our knowledge, this work is the first to demonstrate experimentally (in a quantitative manner) the concerted interactions of copper and cerium in the activation of oxygen and its transfer to carbon monoxide (Figure 5b).

4. CONCLUSIONS

Time-resolved X-ray absorption spectroscopy provides unique insight into the mechanism of oxygen activation on highly dispersed copper-ceria catalysts. A specially designed non-steady-state experimental strategy combined with time-resolved XAS allowed comparing the reactivity of copper and cerium atoms during the CO oxidation cycle. Oxygen activation mediated by a strongly bound oxygen intermediate involves the redox activity of Cu^{2+}/Cu^+ and Ce^{4+}/Ce^{3+} couples. Cu^{2+} and Ce^{4+} reduction rates are kinetically coupled to the rate-determining step of CO oxidation. The extent of participation of the Ce^{4+}/Ce^{3+} couple in CO oxidation is about 10 times lower than that of Cu^{2+}/Cu^+. However, both metals react in concert, likely being a part of the same active site. Long-lived Cu^+ and Ce^{3+} species also appear during the CO oxidation process. While their origin and reactivity require clarification, we prove that they do not activate oxygen to form a strongly bound oxygen intermediate.

■ ASSOCIATED CONTENT

Supporting Information

The Supporting Information is available free of charge at https://pubs.acs.org/doi/10.1021/acscatal.0c00551.

Analysis methods of time-resolved XAS data, results of EXAFS data analysis, concentrations of Cu^+ and Ce^{3+} and activity data and corresponding rates obtained from time-resolved XAS experiments, kinetics of gas exchange in the experimental cell, EXAFS fits at the Cu K edge, TEM images of 4 wt % Cu-CeO_2 catalyst, evolution of CO_2 concentration in 1% CO after oxygen cutoff, evolution of CO conversion and changes in the catalyst bed temperature during oxygen cutoff experiments, long-term decay of CO_2 conversion after switching on the oxygen supply, comparison of Cu K edge XANES spectra of the catalyst in the oxidized state, results of PCA analysis on Cu K edge XANES, linear correlation between Cu K-edge XANES and Cu^+ concentration, Ce L_3 XANES spectra of 4 wt % Cu-CeO_2 catalyst with those of the reference samples, and evolution of Cu^+ concentration in 4 wt % Cu-CeO_2 catalyst during the first cycle of an oxygen-cutoff experiment at different temperatures (PDF)

■ AUTHOR INFORMATION

Corresponding Author

Olga V. Safonova − *Paul Scherrer Institute, 5232 Villigen PSI, Switzerland;* orcid.org/0000-0002-6772-1414; Email: olga.safonova@psi.ch

Authors

Alexander Guda − *The Smart Materials Research Institute, Southern Federal University, Rostov-on-Don 344090, Russian Federation*

https://dx.doi.org/10.1021/acscatal.0c00551
ACS Catal. 2020, 10, 4692−4701

Yury Rusalev − *The Smart Materials Research Institute, Southern Federal University, Rostov-on-Don 344090, Russian Federation*
René Kopelent − *Paul Scherrer Institute, 5232 Villigen PSI, Switzerland*
Grigory Smolentsev − *Paul Scherrer Institute, 5232 Villigen PSI, Switzerland*
Wey Yang Teoh − *School of Chemical Engineering, The University of New South Wales, Sydney, New South Wales 2052, Australia;* orcid.org/0000-0002-4400-4578
Jeroen A. van Bokhoven − *Paul Scherrer Institute, 5232 Villigen PSI, Switzerland; Institute for Chemistry and Bioengineering, ETH Zurich, 8093 Zürich, Switzerland;* orcid.org/0000-0002-4166-2284
Maarten Nachtegaal − *Paul Scherrer Institute, 5232 Villigen PSI, Switzerland;* orcid.org/0000-0003-1895-9626

Complete contact information is available at: https://pubs.acs.org/10.1021/acscatal.0c00551

Author Contributions

W.Y.T. prepared and characterized the catalyst. R.K. and Y.R. performed the ex situ catalytic tests. A.G., O.V.S., and R.K. performed in situ/operando XAS experiments and analyzed the results. O.V.S. and A.G. designed the experiments. G.S. contributed to the development of the fluorescence detected time-resolved XAS method. O.V.S. supervised the project. All authors were involved in the discussion of the results and writing of the manuscript. All authors have given approval to the final version of the manuscript.

Notes

The authors declare no competing financial interest.

■ ACKNOWLEDGMENTS

We thank Dr. Frank Krumeich from ETH Zurich for detailed STEM analysis of the catalyst and help with the interpretation of the results. We thank Dr. Davide Ferri, Dr. Vitaly Sushkevich, and Dr. Maxim Zabilskiy (Paul Scherrer Institute) for fruitful discussions. We thank J. Imbao and D. Kuzmenko (Paul Scherrer Institute) for help during beamtimes. We thank the Swiss Light Source for granting beamtime at the SuperXAS beamline. We gratefully acknowledge financial support for O.V.S. and R.K. from the Swiss National Science Foundation Grant No. 200021_140750. Y.R. acknowledges the Russian Science Foundation project No. 17-72-10245 for travel support. A.G. acknowledges the President's Grant of Russian Federation for young scientists MK-2730.2019.2.

■ REFERENCES

(1) Konsolakis, M. The Role of Copper−Ceria Interactions in Catalysis Science: Recent Theoretical and Experimental Advances. *Appl. Catal., B* **2016**, *198*, 49−66.
(2) Li, Y.; Fu, Q.; Flytzani-Stephanopoulos, M. Low-Temperature Water-Gas Shift Reaction over Cu- and Ni-Loaded Cerium Oxide Catalysts. *Appl. Catal., B* **2000**, *27* (3), 179−191.
(3) Chen, A.; Yu, X.; Zhou, Y.; Miao, S.; Li, Y.; Kuld, S.; Sehested, J.; Liu, J.; Aoki, T.; Hong, S.; Camellone, M. F.; Fabris, S.; Ning, J.; Jin, C.; Yang, C.; Nefedov, A.; Wöll, C.; Wang, Y.; Shen, W. Structure of the Catalytically Active Copper−Ceria Interfacial Perimeter. *Nat. Catal.* **2019**, *2* (4), 334.
(4) Graciani, J.; Mudiyanselage, K.; Xu, F.; Baber, A. E.; Evans, J.; Senanayake, S. D.; Stacchiola, D. J.; Liu, P.; Hrbek, J.; Sanz, J. F.; Rodriguez, J. A. Highly Active Copper-Ceria and Copper-Ceria-Titania Catalysts for Methanol Synthesis from CO2. *Science* **2014**, *345* (6196), 546−550.
(5) Liu, W.; Flytzanistephanopoulos, M. Total Oxidation of Carbon-Monoxide and Methane over Transition Metal Fluorite Oxide Composite Catalysts: II. Catalyst Characterization and Reaction-Kinetics. *J. Catal.* **1995**, *153* (2), 317−332.
(6) Kašpar, J.; Fornasiero, P.; Hickey, N. Automotive Catalytic Converters: Current Status and Some Perspectives. *Catal. Today* **2003**, *77* (4), 419−449.
(7) Sedmak, G.; Hocevar, S.; Levec, J. Kinetics of Selective CO Oxidation in Excess of H-2 over the Nanostructured Cu0.1Ce0.9O2-(y) Catalyst. *J. Catal.* **2003**, *213* (2), 135−150.
(8) Nagai, Y.; Dohmae, K.; Nishimura, Y. F.; Kato, H.; Hirata, H.; Takahashi, N. Operando XAFS Study of Catalytic NO Reduction over Cu/CeO2: The Effect of Copper−Ceria Interaction under Periodic Operation. *Phys. Chem. Chem. Phys.* **2013**, *15* (22), 8461−8465.
(9) Zabilskiy, M.; Djinović, P.; Tchernychova, E.; Tkachenko, O. P.; Kustov, L. M.; Pintar, A. Nanoshaped CuO/CeO2Materials: Effect of the Exposed Ceria Surfaces on Catalytic Activity in N2O Decomposition Reaction. *ACS Catal.* **2015**, *5* (9), 5357−5365.
(10) Zhang, R.; Teoh, W. Y.; Amal, R.; Chen, B.; Kaliaguine, S. Catalytic Reduction of NO by CO over Cu/CexZr1−xO2 Prepared by Flame Synthesis. *J. Catal.* **2010**, *272* (2), 210−219.
(11) Tschöpe, A.; Markmann, J.; Zimmer, P.; Birringer, R. Chadwick. N2O Temperature-Programmed Oxidation and EXAFS Studies on the Dispersion of Copper in Ceria-Supported Nanocatalysts. *Chem. Mater.* **2005**, *17* (15), 3935−3943.
(12) Kydd, R.; Teoh, W. Y.; Wong, K.; Wang, Y.; Scott, J.; Zeng, Q.-H.; Yu, A.-B.; Zou, J.; Amal, R. Flame-Synthesized Ceria-Supported Copper Dimers for Preferential Oxidation of CO. *Adv. Funct. Mater.* **2009**, *19* (3), 369−377.
(13) Martínez-Arias, A.; Fernández-García, M.; Gálvez, O.; Coronado, J. M.; Anderson, J. A.; Conesa, J. C.; Soria, J.; Munuera, G. Comparative Study on Redox Properties and Catalytic Behavior for CO Oxidation of CuO/CeO2 and CuO/ZrCeO4 Catalysts. *J. Catal.* **2000**, *195* (1), 207−216.
(14) Harrison, P. G.; Ball, I. K.; Azelee, W.; Daniell, W.; Goldfarb, D. Nature and Surface Redox Properties of Copper(II)-Promoted Cerium(IV) Oxide CO-Oxidation Catalysts. *Chem. Mater.* **2000**, *12*, 3715.
(15) Gamarra, D.; Fernández-García, M.; Belver, C.; Martínez-Arias, A. Operando DRIFTS and XANES Study of Deactivating Effect of CO2 on a Ce0.8Cu0.2O2 CO-PROX Catalyst. *J. Phys. J. Phys. Chem. C* **2010**, *114* (43), 18576−18582.
(16) Wang, F.; Büchel, R.; Savitsky, A.; Zalibera, M.; Widmann, D.; Pratsinis, S. E.; Lubitz, W.; Schüth, F. In Situ EPR Study of the Redox Properties of CuO−CeO2 Catalysts for Preferential CO Oxidation (PROX). *ACS Catal.* **2016**, *6* (6), 3520−3530.
(17) Kydd, R.; Ferri, D.; Hug, P.; Scott, J.; Teoh, W. Y.; Amal, R. Temperature-Induced Evolution of Reaction Sites and Mechanisms during Preferential Oxidation of CO. *J. Catal.* **2011**, *277* (1), 64−71.
(18) Elias, J. S.; Artrith, N.; Bugnet, M.; Giordano, L.; Botton, G. A.; Kolpak, A. M.; Shao-Horn, Y. Elucidating the Nature of the Active Phase in Copper/Ceria Catalysts for CO Oxidation. *ACS Catal.* **2016**, *6* (3), 1675−1679.
(19) Bu, Y.; Er, S.; Niemantsverdriet, J. W. H.; Fredriksson, H. O.A. Preferential Oxidation of CO in H2 on Cu and Cu/CeOx Catalysts Studied by in Situ UV−Vis and Mass Spectrometry and DFT. *J. Catal.* **2018**, *357*, 176−187.
(20) Monte, M.; Munuera, G.; Costa, D.; Conesa, J. C.; Martinez-Arias, A. Near-Ambient XPS Characterization of Interfacial Copper Species in Ceria-Supported Copper Catalysts. *Phys. Chem. Chem. Phys.* **2015**, *17* (44), 29995−30004.
(21) Polster, C. S.; Nair, H.; Baertsch, C. D. Study of Active Sites and Mechanism Responsible for Highly Selective CO Oxidation in H2 Rich Atmospheres on a Mixed Cu and Ce Oxide Catalyst. *J. Catal.* **2009**, *266* (2), 308−319.
(22) Moreno, M.; Bergamini, L.; Baronetti, G. T.; Laborde, M. A.; Mariño, F. J. Mechanism of CO Oxidation over CuO/CeO2 Catalysts. *Int. J. Hydrogen Energy* **2010**, *35* (11), 5918−5924.

(23) Sedmak, G.; Hočevar, S.; Levec, J. Transient Kinetic Model of CO Oxidation over a Nanostructured Cu0.1Ce0.9O2−y Catalyst. *J. Catal.* **2004**, *222* (1), 87−99.
(24) Baber, A. E.; Yang, X.; Kim, H. Y.; Mudiyanselage, K.; Soldemo, M.; Weissenrieder, J.; Senanayake, S. D.; Al-Mahboob, A.; Sadowski, J. T.; Evans, J.; Rodriguez, J. A.; Liu, P.; Hoffmann, F. M.; Chen, J. G.; Stacchiola, D. J. Stabilization of Catalytically Active Cu+ Surface Sites on Titanium−Copper Mixed-Oxide Films. *Angew. Chem., Int. Ed.* **2014**, *53* (21), 5336−5340.
(25) Yang, X.; Kattel, S.; Xiong, K.; Mudiyanselage, K.; Rykov, S.; Senanayake, S. D.; Rodriguez, J. A.; Liu, P.; Stacchiola, D. J.; Chen, J. G. Direct Epoxidation of Propylene over Stabilized Cu+ Surface Sites on Titanium-Modified Cu2O. *Angew. Chem., Int. Ed.* **2015**, *54* (41), 11946−11951.
(26) Gamarra, D.; Belver, C.; Fernández-García, M.; Martínez-Arias, A. Selective CO Oxidation in Excess H2 over Copper−Ceria Catalysts: Identification of Active Entities/Species. *J. Am. Chem. Soc.* **2007**, *129* (40), 12064−12065.
(27) Yao, S.; Mudiyanselage, K.; Xu, W.; Johnston-Peck, A. C.; Hanson, J. C.; Wu, T.; Stacchiola, D.; Rodriguez, J. A.; Zhao, H.; Beyer, K. A.; Chapman, K. W.; Chupas, P. J.; Martínez-Arias, A.; Si, R.; Bolin, T. B.; Liu, W.; Senanayake, S. D. Unraveling the Dynamic Nature of a CuO/CeO2 Catalyst for CO Oxidation in Operando: A Combined Study of XANES (Fluorescence) and DRIFTS. *ACS Catal.* **2014**, *4* (6), 1650−1661.
(28) Elias, J. S.; Stoerzinger, K. A.; Hong, W. T.; Risch, M.; Giordano, L.; Mansour, A. N.; Shao-Horn, Y. In Situ Spectroscopy and Mechanistic Insights into CO Oxidation on Transition-Metal-Substituted Ceria Nanoparticles. *ACS Catal.* **2017**, *7* (10), 6843−6857.
(29) Oyama, S. T.; Li, W. Absolute Determination of Reaction Mechanisms by in Situ Measurements of Reaction Intermediates. *Top. Catal.* **1999**, *8* (1−2), 75−80.
(30) Kopelent, R.; van Bokhoven, J. A.; Szlachetko, J.; Edebeli, J.; Paun, C.; Nachtegaal, M.; Safonova, O. V. Catalytically Active and Spectator Ce3+ in Ceria-Supported Metal Catalysts. *Angew. Chem., Int. Ed.* **2015**, *54* (30), 8728−8731.
(31) Kopelent, R.; van Bokhoven, J. A.; Nachtegaal, M.; Szlachetko, J.; Safonova, O. V. X-Ray Emission Spectroscopy: Highly Sensitive Techniques for Time-Resolved Probing of Cerium Reactivity under Catalytic Conditions. *Phys. Chem. Chem. Phys.* **2016**, *18* (47), 32486−32493.
(32) Chiarello, G. L.; Nachtegaal, M.; Marchionni, V.; Quaroni, L.; Ferri, D. Adding Diffuse Reflectance Infrared Fourier Transform Spectroscopy Capability to Extended X-Ray-Absorption Fine Structure in a New Cell to Study Solid Catalysts in Combination with a Modulation Approach. *Rev. Sci. Instrum.* **2014**, *85* (7), No. 074102.
(33) Guda, A. A.; Bugaev, A. L.; Kopelent, R.; Braglia, L.; Soldatov, A. V.; Nachtegaal, M.; Safonova, O. V.; Smolentsev, G. Fluorescence-Detected XAS with Sub-Second Time Resolution Reveals New Details about the Redox Activity of Pt/CeO2 Catalyst. *J. Synchrotron Radiat.* **2018**, *25* (4), 989.
(34) Smolentsev, G.; Soldatov, A. V. FitIt: New Software to Extract Structural Information on the Basis of XANES Fitting. *Comput. Mater. Sci.* **2007**, *39* (3), 569−574.
(35) Smolentsev, G.; Guilera, G.; Tromp, M.; Pascarelli, S.; Soldatov, A. V. Local Structure of Reaction Intermediates Probed by Time-Resolved x-Ray Absorption near Edge Structure Spectroscopy. *J. Chem. Phys.* **2009**, *130* (17), 174508.
(36) Ravel, B.; Newville, M. ATHENA, ARTEMIS, HEPHAESTUS: Data Analysis for X-Ray Absorption Spectroscopy Using IFEFFIT. *J. Synchrotron Radiat.* **2005**, *12* (4), 537−541.
(37) Zhang, R.; Miller, J. T.; Baertsch, C. D. Identifying the Active Redox Oxygen Sites in a Mixed Cu and Ce Oxide Catalyst by in Situ X-Ray Absorption Spectroscopy and Anaerobic Reactions with CO in Concentrated H2. *J. Catal.* **2012**, *294*, 69−78.
(38) Elias, J. S.; Stoerzinger, K. A.; Hong, W. T.; Risch, M.; Giordano, L.; Mansour, A. N.; Shao-Horn, Y. In Situ Spectroscopy and Mechanistic Insights into CO Oxidation on Transition-Metal-Substituted Ceria Nanoparticles. *ACS Catal.* **2017**, *7*, 6843.
(39) Wang, X.; Rodriguez, J. A.; Hanson, J. C.; Gamarra, D.; Martínez-Arias, A.; Fernández-García, M. Unusual Physical and Chemical Properties of Cu in Ce1-XCuxO2 Oxides. *J. Phys. Chem. B* **2005**, *109* (42), 19595−19603.
(40) Lockard, J. V.; Kabehie, S.; Zink, J. I.; Smolentsev, G.; Soldatov, A.; Chen, L. X. Influence of Ligand Substitution on Excited State Structural Dynamics in Cu(I) Bisphenanthroline Complexes. *J. Phys. Chem. B* **2010**, *114* (45), 14521−14527.
(41) Avgouropoulos, G.; Ioannides, T. Adsorption and Reaction of CO on CuO−CeO2 Catalysts Prepared by the Combustion Method. *Catal. Lett.* **2007**, *116* (1), 15−22.
(42) Avgouropoulos, G.; Ioannides, T. TPD and TPSR Study of CO Interaction with CuO−CeO2 Catalysts. *J. Mol. Catal. A: Chem.* **2008**, *296* (1), 47−53.
(43) Goguet, A.; Meunier, F. C.; Tibiletti, D.; Breen, J. P.; Burch, R. Spectrokinetic Investigation of Reverse Water-Gas-Shift Reaction Intermediates over a Pt/CeO2 Catalyst. *J. Phys. Chem. B* **2004**, *108* (52), 20240−20246.
(44) Safonova, O. V.; Guda, A. A.; Paun, C.; Smolentsev, N.; Abdala, P. M.; Smolentsev, G.; Nachtegaal, M.; Szlachetko, J.; Soldatov, M. A.; Soldatov, A. V.; van Bokhoven, J. A. Electronic and Geometric Structure of Ce3+ Forming Under Reducing Conditions in Shaped Ceria Nanoparticles Promoted by Platinum. *J. Phys. Chem. C* **2014**, *118* (4), 1974−1982.
(45) Luo, M.-F.; Zhong, Y.-J.; Yuan, X.-X.; Zheng, X.-M. TPR and TPD Studies of CuOCeO2 Catalysts for Low Temperature CO Oxidation. *Appl. Catal., A* **1997**, *162* (1), 121−131.

https://dx.doi.org/10.1021/acscatal.0c00551
ACS Catal. 2020, 10, 4692−4701